



# Contact characteristics of cycloid planetary gear drives considering backlashes and clearances

Ling-Chiao Chang<sup>1</sup> · Shyi-Jeng Tsai<sup>1</sup> · Ching-Hao Huang<sup>2</sup>

Received: 26 March 2021 / Accepted: 4 August 2021 / Published online: 13 September 2021  
© Springer-Verlag GmbH Deutschland, ein Teil von Springer Nature 2021

## Abstract

The cycloid planetary gear reducers in so-called Cyclo-type design are developed for a long time and already used in many applications. However, the analysis of performance under some extreme conditions becomes more important because the demand for accuracy increases. Among them, bearing clearance play a significant role for contact characteristics of the drives. It is not only because the transmission accuracy can be affected, but also because the load capacity of bearings would be reduced accordingly. Because of presence of bearing clearances, the cycloid disc is floating with three degree of freedom in the planar mechanism. This condition will cause more complicate in the load analysis for multiple contact pairs. The aim of the paper is thus to analyse contact characteristics of the relevant contact pairs in the Cyclo-type gear drives considering not only the influences of the crank bearing and the pin-hole clearances, but also profile modification of cycloid flank. A computerized loaded tooth contact analysis (LTCA) approach based on influence coefficient method is proposed in the paper for analysis of Cyclo-type drives having clearances. The effects of the clearances on contact characteristics are afterwards analysed by using an example from industry. The variation of shared load, contact stress on each individual cycloid tooth and on bearing roller, as well as the load of pin-hole are simulated with comparison of three different amounts of bearing clearance. The results show that the bearing clearances affect the loads acting on the pins of the pin-shaft more strongly than the bearing, and have almost no significant influence on the contact with the pins of the pin wheel. The pin-hole clearance has less influences on the acting loads on the contact pairs, but affects significantly the peak-to-peak value of transmission errors.

---

✉ Shyi-Jeng Tsai  
sjtsai@cc.ncu.edu.tw

<sup>1</sup> Department of Mechanical Engineering, National Central University, No. 300, Jhong-Da Road, Jhong-Li District, Taoyuan 320, Taiwan

<sup>2</sup> Transmission Machinery Co., Ltd., No. 17, Aly. 31, Lane 69, Xingnong Road, Shanhua Dist., Tainan 741, Taiwan

## Kontakteigenschaften von Zykloiden-Planetengetrieben unter Berücksichtigung von Spiel und Lagerluft

### Zusammenfassung

Die Zykloiden-Planetengetriebe in sogenannter Cyclo-Bauweise werden seit langem entwickelt und bereits in vielen Anwendungen eingesetzt. Die Analyse der Leistung unter einigen extremen Bedingungen wird jedoch wichtiger, da die Anforderungen an die Genauigkeit steigen. Unter anderem spielt die Lagerluft eine wesentliche Rolle für die Kontakteigenschaften der Antriebe. Dies liegt nicht nur daran, dass die Übertragungsgenauigkeit beeinträchtigt werden kann, sondern auch, weil die Tragfähigkeit der Lager entsprechend reduziert wird. Wegen des Vorhandenseins von Lagerluft schwebt die Zykloidscheibe mit drei Freiheitsgraden im planaren Getriebe. Diese Bedingung wird die Lastanalyse für mehrere Kontaktpaare komplizierter machen. Ziel der Arbeit ist es daher, die Kontakteigenschaften der relevanten Kontaktpaare in den Zykloidengetrieben unter Berücksichtigung der Einflüsse der Kurbellagerlüfte und der Bolzen-Bohrung-Spiele, aber auch der Profilmodifikation der Zykloidenflanke zu analysieren. Ein computergestützter belasteter Kontaktanalyse Ansatz auf der Grundlage eines Einflusskoeffizientenverfahrens wird in diesem Artikel zur Analyse von Cyclo-Antrieben mit Spiel und Lagerluft vorgeschlagen. Die Auswirkungen von Lagerluft und Spiel auf die Kontakteigenschaften werden anschließend anhand eines Beispiels aus der Industrie analysiert. Die Variation der geteilten Belastung, der Kontaktspannung an jedem einzelnen Zykloidenzahn und an der Lagerrolle sowie die Belastung der Bolzen-Bohrung werden durch den Vergleich von drei verschiedenen Lagerluftgrößen simuliert. Die Ergebnisse zeigen, dass die Lagerluft die auf die Zapfen der Zapfenwelle wirkenden Belastungen stärker beeinflussen als das Lager und den Kontakt mit den Triebstockverzahnung des Innenrades fast nicht wesentlich beeinflussen. Das Pin-Bohrung-Spiel hat weniger Einfluss auf die einwirkenden Belastungen der Kontaktpaare, beeinflusst aber maßgeblich den Spitze-Tal-Wert von Übertragungsfehlern.

### 1 Introduction

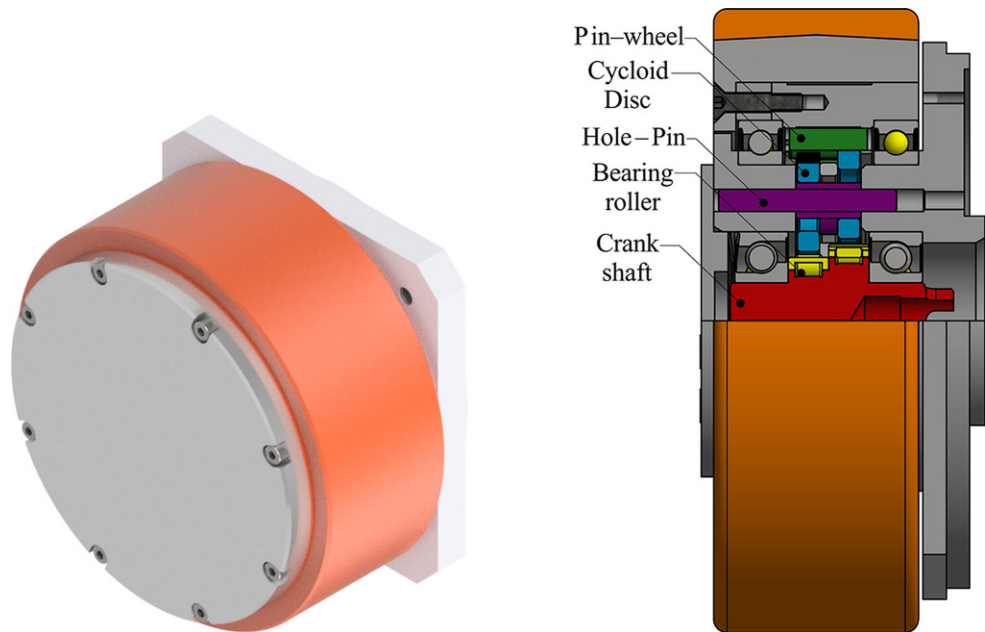
In general, the cycloid planetary gear reducers can be divided into two different types of design, so-called Cyclo-type and RV-type. The Cyclo reducer [2] is characterized by two coaxial components, i.e. the crank and the pin-wheel, one or two cycloid discs as planets, as well as a special output mechanism. This output mechanism is usually designed as a pin-hole parallel mechanism with a ratio  $i = +1$  to convert the rotational motion from the eccentrically mounted cycloid disc to the coaxial transmission of the low-speed pin-shaft. The RV-reducer, on the other hand, combines a planetary gear stage and a cycloid gear stage. It consists of three coaxial components, i.e., a sun gear of planetary stage, a pin-wheel of cycloid stage, as well as a planetary carrier for both stages. The eccentric motion of the cycloid disc is realized by two or three cranks which are connected with the planet gears. The common advantages of the two types of gear reducers are high gear ratio and high ability to absorb impact. In general, RV-reducers have less backlash and larger stiffness than Cyclo-reducer. However, Cyclo-reducers have lower manufacturing cost and more compact design than RV-reducers. Therefore, Cyclo-reducers are widely used in the application where lower precision and frequent reverse motion are required. One of the practical examples is the wheel gearbox of automatic guided vehicles (AGV), see Fig. 1.

In order to achieve higher performance, the analysis of the cycloid gear drive to select suitable parameters is essential. This analysis work is mostly carried out under ideal

conditions. If manufacturing and assembly errors are considered to simulate the performances under actual conditions, the backlash between the teeth, the clearances in the crank-bearing and the output mechanism cannot be ignored. In particular, the contact characteristics, such as the unloaded/loaded transmission errors, the shared loads and the contact stress on each individual contact pairs in the drive are affected strongly by the backlash and the clearances. As a consequence, service life of the main components like crank-bearings or cycloid flanks/pins will be reduced. However, the load analysis for multiple contact pairs becomes more complicate in such the actual situation, i.e., in presence of bearing clearances, because the cycloid disc is floating with three degrees of freedom in planar kinematics. Among the various types of contact pairs in the Cyclo-reducer, the contact of bearing rollers is the most significant.

There are many bearing models for solving the bearing loads with clearance, such as static bearing model, quasi-static bearing model and numerical approach [3]. In the significance reference book [4], Harris offered useful principles for designing rolling bearings. The essential relation for calculating loads in rolling bearing elements with bearing clearances under external loads are also provided for reference. Ji [5] derived a static bearing analysis model based on Stribeck's model and simulated contact stress between rollers and raceways with considering errors of roller diameter. Filetti [6] studied on bearing load distribution based on Jone's contact model, and built a mathematical model of outer race and fixed structure that are simplified in elementary beams for application in finite element method.

**Fig. 1** AGV with Cyclo-type gear drive [1]



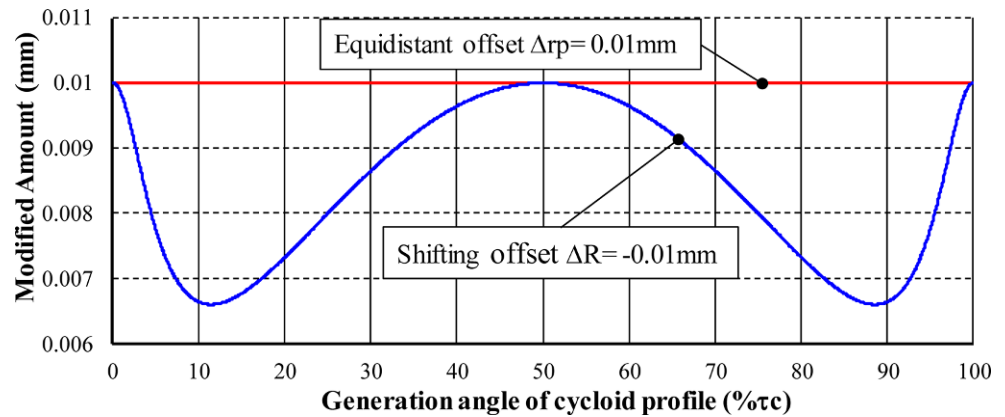
The bearing load can be exactly calculated with considering structural deformations and the results were also verified by experiment. Bourdon [7] established finite element method by introducing stiffness matrices based on Hertzian hypotheses to simulate the bearing nonlinear static behaviour with variation of bearing clearance and other factors. Szuminski [8] built an analysis model for bearing roller based on the Hertzian contact theory to determine the radial and axial stiffness of rolling bearing that relate to adjustable external load and the kinematic characteristic. Edwin [9] applied a numerical approach in mechanical event simulation based on the Harris-Jones model to analyse the contact loading of cylindrical roller bearing with different load types on shaft. Qian [10] used software SIMPACK to study the dynamic behaviours of cylindrical roller bearings due to the influence of cage center orbit with different clearances. Unlike the models mentioned above, Kabus [11] established a six-dof model of roller contact based on non-Hertzian theory so as to analyse tapered roller bearings with considering profile modification of rollers and axis misalignment.

Additionally, modelling the cycloid gear drive with considering bearing clearance is an essential study. Xu [12] established a dynamic model for Cyclo-type gear drive without considering bearing clearance. The analysis results show that the presence of bearing does not affect the loaded contact characteristics of cycloid tooth pairs. Apart from this research, Xu [13] also proposed a dynamic contact model for RV-type gear reducer with considering bearing clearance. The results reveal that the bearing load will increase and the contact force on pin-wheel decreases in most rotation angle of the crank shaft if the radial bearing clearances are present. According to the principle from Harris,

Huang [14] proposed an optimization approach considering bearing clearance for the RV-type gear drive, so as to evaluate the modified parameters of roller profiles for better fatigue life of the crank bearing.

The aim of the paper is to analyse the contact characteristics of the relevant contact pairs in the “Cyclo-type” gear reducer considering the effects of backlashes and clearances. A new LTCA model is expanded from the developed model proposed in the previous study [15–18]. Three contact pairs are included herein: the pairs of the cycloid flank with the pins of pin-wheel, the pairs of the crank bearing rollers and the inner/outer race, as well as the pairs of the holes on cycloid disc and the pins of the pin shaft. Not only the clearances or the backlashes, but also the profile modification of the cycloid flank are also considered in this model. An algorithm for iterative calculation is developed to solve the contact problem of the floating cycloid disc due to the clearances, where the final position of the cycloid disc and the angular displacement of the crank are the variables for convergence. An example from industry is studied in the paper using the proposed approach. Besides the transmission errors, the variation of the shared load and the contact stress on each individual contact pairs are afterwards simulated considering the influences of different values of clearance. The influences of clearances on the contact characteristics are studied systematically. Some findings from the influence analysis results of clearances are given.

**Fig. 2** Modification amount for single cycloid tooth



## 2 Fundamentals for the cycloid gear drive

The contact analysis of the cycloid gear drive having relevant clearances is based on the analysis methods under the clearance-free condition. Related theoretical relations of the model are introduced as follows.

### 2.1 Equations of the modified cycloid tooth profile

The flank modification of cycloid gear is necessary to form the backlash in the cycloid gear drive. From the equations of theoretical cycloid tooth profile [15–18], the cycloid flank can be modified by the variation of the pin-wheel radius  $r_P$  and the pitch circle radius  $R_C$  of the pin-wheel, i.e., so-called equidistant offset and shifting offset modification types, respectively, as shown in Fig. 2.

The equations of modified cycloid tooth profile can be expressed as the equation [18]:

$$r_C(\theta) = (R_C + \Delta R_C) \cdot e^{i\theta} - e \cdot e^{i(i_C \cdot \theta)} - (r_P + \Delta r_P) \cdot e^{i(\theta + \psi(\theta))} \tag{1}$$

### 2.2 Tooth contact analysis (TCA)

The first step to analyze the contact characteristics of the cycloid gear drive is to determine the positions of the contact points of the cycloid disc with the pin-wheel, the pin-shaft and the bearing rollers, as well as the corresponding transmission errors.

#### 2.2.1 Pin-wheel contact conditions

The meshing relation is based on the relative motion of the cycloid disc and each pin. As the relation shown in Fig. 3, the cycloid disc is regarded as stationary, the pin-wheel revolves relatively around the center of cycloid disc with the angle  $\varphi_C$ , and also rotates around its center  $O_{CA,0}$  with an angle  $\varphi_P (= \varphi_C / u)$ . Each pin  $i$  contacts the cycloid

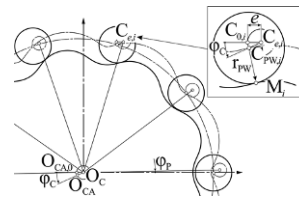


**Fig. 3** Determination of the contact point of the modified cycloid profile with the pin ( $\varphi_P$  is given)

flank at point  $M_{PW_i}$ . The position of each pin can be thus defined by two conditions due to the relative motion of the pin-wheel:

- *The locus due to the revolution.* The center  $C_{PW_i}$  of each pin moves in a circle with a radius  $e$  (equal to eccentricity of the crank) around the center  $C_{ci}$  due to the revolution of the pin-wheel.
- *The locus due to the tangency condition of contact.* The center  $C_{PW_i}$  of each pin must locate on the equidistant curve of the cycloid profile with a distance equal to the pin radius  $r_P$  due to the tangency condition of tooth contact.

The contact position of center  $C_{PW_i}$  of pin  $i$  is therefore the intersecting point of both curves mentioned above. If the rotating angle of the pin-wheel  $\varphi_P$  is given, the rotation angle of the crankshafts  $\varphi_{Ci}$  for each pin can be calculated accordingly. In case of modified cycloid profile, however, the angles  $\varphi_{Ci}$  of each pin are not the same. More details can be found in [18].

#### 2.2.2 Hole-pin contact condition

Ideally, each pin of the pin-shaft is located evenly and contacts the pin hole of cycloid disc simultaneously. In general, only a half of pins are in working to transmit the motion. This contact condition can be determined by using two vectors, shown in Fig. 4:

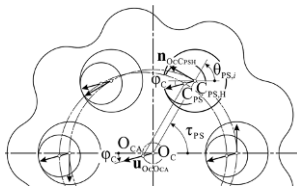


**Fig. 4** Effective contact pair of pin-shaft

- **Normal vector  $\mathbf{n}_{OCCPSH,i}$ :** The normal vector is perpendicular to the center line of the cycloid disc center  $O_C$  and the pin-hole center  $C_{PSH,i}$ . It is defined as:

$$\mathbf{n}_{OCCPSH,i} = [-\sin \theta_{PSH,i}, \cos \theta_{PSH,i}]^T \tag{2}$$

with the corresponding azimuth angle  $\theta_{PSH,i}$ :

$$\theta_{PSH,i} = (i - 1) \cdot \tau_{PS} = (i - 1) \cdot 2\pi/z_{PS} \tag{3}$$

- **Position vector  $\mathbf{u}_{OCAOC}$ :** This vector is defined as the position of the pin center of pin-shaft  $C_{PS,i}$  relative to the pin hole on the cycloid disc  $C_{PSH,i}$ . In error-free case, it is parallel to the position vector of the pin-wheel center  $O_{CA}$  relative to the cycloid disc center  $O_C$ , namely:

$$\mathbf{u}_{OCAOC} = [-\cos(\lambda \cdot \varphi_C), -\sin(\lambda \cdot \varphi_C)]^T \tag{4}$$

where the coefficient  $\lambda$  is equal to +1 when the crank shaft rotates in counterclockwise direction, and -1 for clockwise direction. Pin  $i$  of the pin-shaft is effective for transmission if the inner product of these two vectors is positive, and versa. The effective contact pair of hole-pin can be thus determined accordingly.

### 2.2.3 Roller bearing contact condition

The contact points on bearing rollers can be determined simply based on the geometric relation of the centers of the roller  $C_{BR,i}$  and the inner or outer race  $O_C$ , respectively. Details are not mentioned here. However, it is necessary to determine which roller should be involved into the calculation in order to reduce the calculation time and to increase the calculation accuracy.

With a predicted load  $\mathbf{F}_{predict}$  due to the radial  $\delta_r$  and the tangential  $\delta_t$  displacements of the cycloid disc, the bearing roller within the loaded zone with a range of  $\pm\theta_{predict}$  can be regarded as in contact. Although  $\theta_{predict}$  is  $90^\circ$  for ideal condition, the angle  $\theta_{predict}$  in the paper will be selected as larger than  $90^\circ$  due to deviation of the prediction direction from

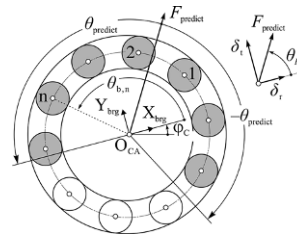


**Fig. 5** Predicting effective contact pairs of rollers

the actual. The condition for effective roller is represented as (Fig. 5):

$$\cos(\theta_{predict}) \leq \cos(\theta_{b,n} - \theta_F) \tag{5}$$

### 2.2.4 Transmission error

In the case of actual condition, the relation between the output and the input rotation angle is not linear any more. For the convenience of analysis in the paper, the transmission error  $TE_{\varphi_C}$  is derived from the difference of actual rotation angle  $\varphi_{C,act}$  and theoretical rotation angle  $\varphi_{C,theor}$  of the crankshaft which is based on the given output rotation angle  $\varphi_P$ .

$$TE_{\varphi_C} = \varphi_{C,act} - \varphi_{C,theor} = \varphi_{C,act} - u \cdot \varphi_{P,given} \tag{6}$$

$TE_{\varphi_C}$  can be also easily converted to  $TE_{\varphi_P}$  on the output side by dividing the gear ratio  $u$ .

### 2.3 Loaded tooth contact analysis (LTCA) model

The LTCA model developed in the study is based on the influence coefficient method and can solve not only the load sharing among the multiple contact tooth pairs, but also the contact stress on the engaged flanks. This model consists of two equation types: equations of deformation-displacement of each contact pair and equations of load equilibrium. Because of linear coefficients in equation, a converted matrix equation is used for calculation, namely:

$$\begin{bmatrix} \mathbf{A} & -\mathbf{I} \\ s\mathbf{J} & 0 \end{bmatrix} \begin{bmatrix} \mathbf{P} \\ \delta \end{bmatrix} = \begin{bmatrix} -\mathbf{H} \\ F \end{bmatrix} \tag{7}$$

More details can be found in the previous works [15–20]. The specific relations for the cycloid gear drive are mentioned as follows.

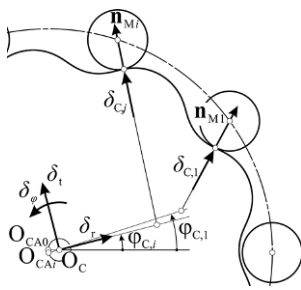


**Fig. 6** Displacement relation of cycloid-pin-shaft contact pairs

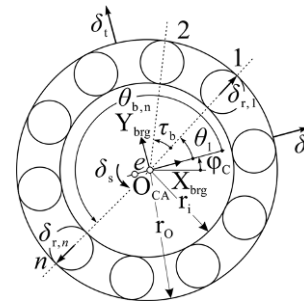


**Fig. 8** Displacement relation of roller bearing

## 2.4 Deformation-displacement relation

### 2.4.1 Cycloid-pinwheel contact pairs

In the case that the supporting bearing for cycloid disc is regarded as flexible, three additional planar displacements of the disc should be considered, i.e. two in translational direction,  $\delta_r$  and  $\delta_t$ , and one in rotational direction  $\delta_\varphi$ . As the relation shows in Fig. 6, the effective displacement  $\delta_{C,j}$  between the contact tooth pair  $i$  along the contact normal can be represented as:

$$\delta_{C,j} = q_{C,r}\delta_r + q_{C,t}\delta_t + q_{C,\varphi}\delta_\varphi \tag{8}$$

The conversion factors,  $q_{C,r}$ ,  $q_{C,t}$ ,  $q_{C,\varphi}$ , are derived from the geometric relation. More details can be found in [16, 17].

### 2.4.2 Cycloid-pin shaft contact pairs

In the error-free case, the deformation  $\delta_{PS,n}$  between the pin  $n$  of the pin-shaft and the pin-hole on the disc is affected by the radial displacement  $\delta_r$  and rotational displacement  $\delta_\varphi$  of the cycloid disc, see Fig. 7:

$$\delta_{PS,n} = -\delta_r + q_{PS,\varphi}\delta_\varphi \tag{9}$$

where the conversion factor  $q_{PS,\varphi}$  of rotation displacement is calculated as:

$$q_{PS,\varphi} = \mathbf{R}_{PSH} \cdot \mathbf{t}_{CPSH} \cdot \mathbf{n}_{CPS} \tag{10}$$

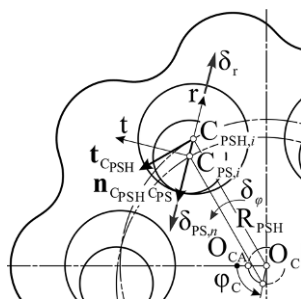


**Fig. 7** Displacement relation of pin-hole contact pairs

### 2.4.3 Cycloid-roller bearing contact pairs

If the translational displacement  $\delta_{C,n}$ , or  $\delta_t$  and  $\delta_r$ , of the cycloid disc are present, the deformation  $\delta_{o,n}$  due to the contact of roller  $n$  with the outer race on the cycloid disc can be determined from the relation in Fig. 8:

$$\delta_{o,n} = \delta_{r,n} - \delta_{C,n} = \delta_{r,n} - q_{B,r}\delta_r - q_{B,t}\delta_t \tag{11}$$

where  $\delta_{r,n}$  is the displacement of bearing roller  $n$  along the direction of contact normal. The conversion factors  $q_{B,r}$  and  $q_{B,t}$  due to the translational displacements of the disc are equal to:

$$q_{B,r} = \cos(\theta_{b,n} - \varphi_C) \tag{12}$$

$$q_{B,t} = \sin(\theta_{b,n} - \varphi_C) \tag{13}$$

The corresponding azimuth angle  $\theta_{b,n}$  of bearing roller in the above equations is affected by the rotation angle of crank shaft  $\varphi_C$ , the radius  $r_i$ ,  $r_o$  of the inner and the outer race, and the number of roller  $n_{BR}$  with the relation:

$$\theta_{b,n} = \theta_{b,1} + \tau_{b,n} = \frac{r_i \cdot \varphi_C}{r_i + r_o} + \frac{2\pi(n-1)}{n_{BR}} \tag{14}$$

### 2.4.4 Crank-Roller bearing contact pairs

Similarly, the deformation  $\delta_{i,n}$  in Fig. 8 due to contact roller  $n$  and the crank is caused by the displacement  $\delta_{r,n}$  of roller  $n$  and the angular displacement  $\delta_s$  of the crank [16]:

$$\delta_{i,n} = \delta_{s,n} - \delta_{r,n} = q_{S,n} \cdot e \cdot \delta_s - \delta_{r,n} \tag{15}$$

where the conversion factor  $q_{S,n}$  for the crank displacement is equal to:

$$q_{S,n} = \sin(\theta_{b,n} - \varphi_C) \tag{16}$$

## 2.5 Flank separation distance of contact tooth pairs

The discrete separation distances between the contact pair are essential in the proposed LTCA for calculation of the



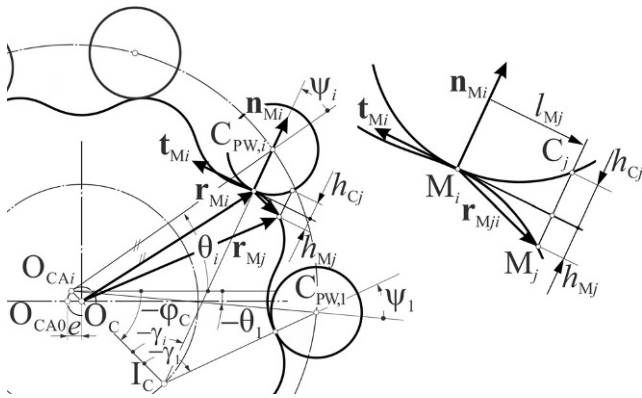


Fig. 9 Flank separation distance relations for cycloid-pinwheel

distributed contact stress. Among the considered contact pairs, the profile of the components, such as the bearing roller, the pin of the pin-wheel and the pin-shaft, is cylindrical. The distance  $h_C$  of a discrete point on the common tangent to the cylindrical profile can be derived from the geometrical relation in Fig. 9:

$$h_C(l) = r - \sqrt{r^2 - l^2} \tag{17}$$

where  $r$  is radius of the cylindrical element, and  $l$  is the distance from the contact point to the discrete point projected on the common tangent plane. On the other hand, the separate distance  $h_{Mj}$  between the contact cycloid flank and the common tangent can be determined from vector calculation with the normal vector  $\mathbf{n}_{Mi}$  and tangential vector  $\mathbf{t}_{Mi}$  on the contact point  $M_i$  and the relative position vector  $\mathbf{r}_{Mji}$  from  $M_j$  to  $M_i$ . With a given distance  $l_{Mj}$ , the position of  $M_j$  can be determined with aid of the equation:

$$\mathbf{r}_{Mji} \cdot \mathbf{t}_{Mi} = l_{Mj} \tag{18}$$

The separation distance  $h_{Mj}$  is then calculated with the determined variable  $\theta$  from Eq. 18 as:

$$h_{Mj} = -\mathbf{r}_{Mji} \cdot \mathbf{n}_{Mi} \tag{19}$$

## 2.6 Load equilibrium relation

### 2.6.1 Cycloid disk

Because the cycloid disc is flexibly supported by the pins of the pin-shaft and the rollers of the crank bearing, the forces from all contact pairs related to the cycloid disc must be in load equilibrium in radial, tangential and rotational direction, respectively (Fig. 10) as the following equations represent.

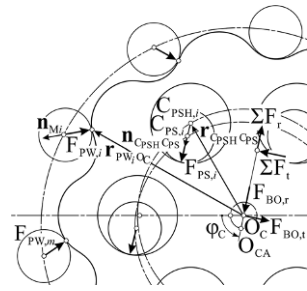


Fig. 10 Load equilibrium relation of cycloid disc

- Force equilibrium in the tangential direction  $\mathbf{t}$ :

$$\sum F_{BO,t} = \sum_i^m [q_{C,ti} \cdot F_{PW_i}] \tag{20}$$

- Force equilibrium in the radial direction,  $\mathbf{r}$ :

$$\sum (q_{C,ri} F_{Ni}) - \lambda \cdot F_{BO,r} - \sum [k_{PS} \cdot (\delta_r - q_{PS,\varphi} \delta_\varphi)] = 0 \tag{21}$$

The Eq. 21 can be simplified as:

$$\sum (q_{C,ri} F_{Ni}) - \lambda \cdot F_{BO,r} + Q_{PS,r} \cdot \delta_r + Q_{PS,\varphi} \cdot \delta_\varphi = 0 \tag{22}$$

The stiffness  $k_{PS}$  of the pin of the pin-shaft is linearized as a constant in the paper.

- Moment equilibrium of cycloid disc: Moment equilibrium of cycloid disc is contributed by the normal forces  $F_{PW}$  acting on the pinwheel and the forces  $F_{PS}$  on pin-shaft, namely:

$$\sum (F_{PW_i} \cdot Q_{MOCPW}) - \sum (F_{PS_i} \cdot Q_{MOCPS}) = 0 \tag{23}$$

The coefficient  $Q_{MOCPW}$  in the above equation is the effective lever arm of the normal forces  $F_{PW}$  relative to the pivot point  $O_C$ , namely determined as:

$$Q_{MOCPW} = |\mathbf{n}_{Mi} \times \mathbf{r}_{PW_i O_C}| \tag{24}$$

Since the force  $F_{PS}$  from the pin-shaft acting on the cycloid disc can be replaced by relative displacements, the equation can be rewritten as:

$$\begin{aligned} & \sum (F_{PW_i} \cdot Q_{MOCPW}) \\ & = \sum (Q_{MOCPS,r} \cdot \delta_r + Q_{MOCPS,\varphi} \cdot \delta_\varphi) \end{aligned} \tag{25}$$

where the coefficient  $Q_{MOCPS}$  is the lever arm of the forces  $F_{PS}$  of the pin-shaft relative to the pivot point  $O_C$ , and can be divided in two directions:

$$Q_{MOCPS,r} = \sum k_{PS} \cdot |\mathbf{r}_{CPSH O_C} \times \mathbf{n}_{CPSH CPS}| \tag{26}$$

$$Q_{MOCPS,\varphi} = - \sum k_{PS} \cdot q_{PS,\varphi} |\mathbf{r}_{CPSH O_C} \times \mathbf{n}_{CPSH CPS}| \tag{27}$$

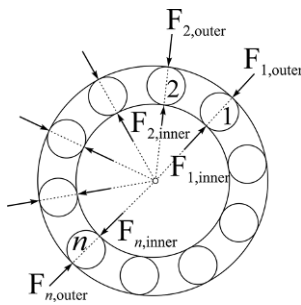


**Fig. 11** Load equilibrium relation of roller bearing

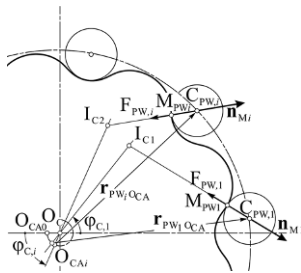


**Fig. 12** Force relation of contact tooth pair with modified cycloid flank for calculating output torque

**2.6.2 Roller bearing**

For each roller  $n$ , the force  $F_{n,outer}$  acting from the cycloid disc must be equal to that from the crank  $F_{n,inner}$  (Fig. 11):

$$F_{n,outer} = F_{n,inner} \tag{28}$$

**2.6.3 Output torque**

The output torque  $T_{out}$  acting on the pin-wheel must be equal to the sum of the moments due to all the individual normal forces  $F_{PW_i}$  on the pin relative to the pivot point  $O_{CA}$  (Fig. 12). The lever arm is calculated by the cross product of the contact normal vector  $\mathbf{n}_{Mi}$  and the position vector of pinwheel  $\mathbf{r}_{PW_iOCA}$ :

$$T_{out} = \sum F_{PW_i} \cdot |\mathbf{n}_{Mi} \times \mathbf{r}_{PW_iOCA}| = \sum F_{PW_i} \cdot Q_{M,PWi} \tag{29}$$

**2.7 LTCA model for cycloid gear drive without clearances**

With the deformation–displacement equations and the load equilibrium equations for all contact tooth pairs derived above, the basic model in Eq. 7 can be rewritten as:

$$\begin{bmatrix} \mathbf{A}_{CD} & \mathbf{0} & \mathbf{0} & \mathbf{q}_{CD} & \mathbf{0} \\ \mathbf{0} & \mathbf{A}_{Brg,O} & \mathbf{0} & \mathbf{q}_{Brg} & \mathbf{C}_{BO} \\ \mathbf{0} & \mathbf{0} & \mathbf{A}_{Brg,I} & \mathbf{0} & \mathbf{q}_{BI} \\ \mathbf{Q}_{CD} & \mathbf{Q}_{Brg} & \mathbf{0} & \mathbf{q}_{PS} & \mathbf{0} \\ \mathbf{J}_{CD} & \mathbf{J}_{Brg,O} & \mathbf{J}_{Brg,I} & \mathbf{0} & \mathbf{0} \end{bmatrix} \begin{bmatrix} \mathbf{P}_{CD} \\ \mathbf{P}_{Brg,O} \\ \mathbf{P}_{Brg,I} \\ \Delta_{CD} \\ \Delta_{Brg} \end{bmatrix} = [-\mathbf{H}_{CD} \quad -\mathbf{H}_{Brg,O} \quad -\mathbf{H}_{Brg,I} \quad \mathbf{0} \quad \mathbf{T}]^T \tag{30}$$

where the representation of each parameter are listed as below.

- The sub-matrix  $\mathbf{q}_{CD}$  and  $\mathbf{q}_{Brg}$  associate with the equivalent coefficients that transform displacements of cycloid disc along the contact normal:

$$\begin{aligned} \mathbf{q}_{CD} &= [\mathbf{q}_{C,r} \quad \mathbf{q}_{C,t} \quad \mathbf{q}_{C,\varphi}] \\ \mathbf{q}_{Brg} &= [\mathbf{q}_{B,r} \quad \mathbf{q}_{B,t} \quad \mathbf{0}] \end{aligned} \tag{31}$$

- The constant matrix  $\mathbf{C}_{BO}$  is equal to:

$$\mathbf{C}_{BO} = [\mathbf{1} \quad \mathbf{0}] \tag{32}$$

- The sub-matrix  $\mathbf{q}_{BI}$  combines the factors that convert displacement of each bearing roller and the crank shaft to the contact normal:

$$\mathbf{q}_{BI} = [-\mathbf{1} \quad \mathbf{q}_{S,n}] \tag{33}$$

- The sub-matrix  $\mathbf{Q}_{CD}$  integrate the matrixes to calculate load equilibrium of the cycloid disc:

$$\mathbf{Q}_{CD} = \begin{bmatrix} \mathbf{Q}_{r,CD} & \mathbf{Q}_{r,Brg} & \mathbf{0} \\ \mathbf{Q}_{t,CD} & \mathbf{Q}_{t,Brg} & \mathbf{0} \\ \mathbf{Q}_{\varphi,CD} & \mathbf{0} & \mathbf{0} \end{bmatrix} \tag{34}$$

- The sub-matrix  $\mathbf{q}_{PS}$  collects the coefficients related to the pin-shaft for load equilibrium calculation of the cycloid disc:

$$\mathbf{q}_{PS} = \begin{bmatrix} \mathbf{Q}_{PS,r} & \mathbf{0} & \mathbf{Q}_{PS,\varphi} \\ \mathbf{0} & \mathbf{0} & \mathbf{0} \\ \mathbf{Q}_{MOCPS,r} & \mathbf{0} & \mathbf{Q}_{MOCPS,\varphi} \end{bmatrix} \tag{35}$$

- The sub-matrix  $\mathbf{J}_{CD}$  is used for calculation of torque equilibrium of output condition:

$$\mathbf{J}_{CD} = [\mathbf{0} \quad \mathbf{Q}_{M,PW}]^T \tag{36}$$

- The sub-matrix  $\mathbf{J}_{Brg,O}$  and  $\mathbf{J}_{Brg,I}$  are the matrixes for calculation of load equilibrium of bearing rollers:

$$\begin{aligned} \mathbf{J}_{Brg,O} &= [\mathbf{S}_{Brg,O} \quad \mathbf{0}]^T \\ \mathbf{J}_{Brg,I} &= [\mathbf{S}_{Brg,I} \quad \mathbf{0}]^T \end{aligned} \tag{37}$$

- The sub-matrix  $\Delta_{CD}$  collects three displacements of cycloid gear:

$$\Delta_{CD} = [\delta_r \quad \delta_t \quad \delta_\varphi]^T \tag{38}$$



- The sub-matrix  $\Delta_{BR}$  collects the displacements of bearing roller and the angular displacement of the crank shaft:

$$\Delta_{BR} = [\Delta_{r,n} \quad \delta_S]^T \tag{39}$$

- The sub-matrix  $\mathbf{T}$  is the boundary condition of the gear drive:

$$\mathbf{T} = [\mathbf{0} \quad T_{out}]^T \tag{40}$$

The matrix can be solved by using LU-decomposition method effectively. The solving process will be iteratively repeated until all the stress is calculated as positive [17, 18].

### 3 Analysis model for cycloid gear drives considering relevant clearances

#### 3.1 Modified LTCA model

Considering the cycloid gear drive as a planar mechanism, the cycloid disc owns three degrees of freedom in presence of tooth pair backlash, bearing clearances and/or hole-pin clearances. As a consequence, the contact position of each element under static condition cannot be determined by using TCA approach mentioned above. However, the deformation of each contact pair in the LTCA model mentioned in Sect. 2 is derived exactly from the contact position and the equivalent displacements. Therefore, the LTCA model must be modified for the case of relevant clearances.

The concept based on determination of the final positions of all contact pairs in load equilibrium is considered in the modified model. Those positions are affected by the four forced displacements, i.e., the tangential  $\delta_i$ , the radial  $\delta_r$ , and the rotational displacement  $\delta_{qCD}$  of the cycloid disc, and the rotational displacement  $\delta_{qC}$  of the crank. The deformation can be regarded as the interference of each contact pair at the final position. As described above, the LTCA model in Eq. 30 is composed of the relations of deformation-displacement and the equations of load equilibrium. Because the four forced displacements are guess values, the relations of load equilibrium related to the forced displacements are removed from the matrix in Eq. 30, and chosen as the convergence criterions for iterative calculation.

As a consequence, the loads  $\mathbf{P}_{CD}$  on the contact pairs of cycloid-pin wheel and the loads  $\mathbf{P}_{Brg,O}$  and  $\mathbf{P}_{Brg,I}$  on the contact pairs related to the bearing rollers can be calculated independently by using the four unknown displacements as guess values, namely:

$$\mathbf{A}_{CD} \cdot \mathbf{P}_{CD} = -\mathbf{H}_{CD,BC} \tag{41}$$

$$\begin{bmatrix} \mathbf{A}_{Brg,O} & \mathbf{0} & \mathbf{1} \\ \mathbf{0} & \mathbf{A}_{Brg,I} & -\mathbf{1} \\ \mathbf{S}_{Brg,O} & \mathbf{Q}_{Brg,I} & \mathbf{0} \end{bmatrix} \begin{bmatrix} \mathbf{P}_{Brg,O} \\ \mathbf{P}_{Brg,I} \\ \Delta_{r,n} \end{bmatrix} = \begin{bmatrix} -\mathbf{H}_{Brg,O-BC} \\ -\mathbf{H}_{Brg,I-BC} \\ \mathbf{0} \end{bmatrix} \tag{42}$$

The required equations of load equilibrium are thus checked if fulfilled or not. The sum of the loads in each direction can be calculated by using the matrix equation:

$$\begin{bmatrix} F_{CY,r} \\ F_{CY,t} \\ M_{OC} \\ T_{PW,Op} \end{bmatrix} = \begin{bmatrix} \mathbf{S}_{CD,r} & \mathbf{S}_{Brg,r} & k_{PS} \\ \mathbf{S}_{CD,t} & \mathbf{S}_{Brg,t} & k_{PS} \\ \mathbf{S}_{CD,M} & \mathbf{0} & k_{PS} \\ \mathbf{S}_{CD,T} & \mathbf{0} & 0 \end{bmatrix} \begin{bmatrix} \mathbf{P}_{CD} \\ \mathbf{P}_{Brg,O} \\ \delta_{intPS,i} \end{bmatrix} \tag{43}$$

The convergence conditions are thus:

$$\begin{aligned} |F_{CY,r}| < \varepsilon_r, \quad |F_{CY,t}| < \varepsilon_t, \\ |M_{OC}| < \varepsilon_\varphi, \quad |T_{PW,Op} - T_{out}| < \varepsilon_T \end{aligned} \tag{44}$$

where the deviation values  $\varepsilon$  are small so as acceptable. If the convergence criterion is not met, a set of new guess values are given. Those displacements are solved then iteratively. The loads and the contact positions of each component can be also determined accordingly. The detailed derivation of the parameters mentioned above will be explained in the subsequent sections.

#### 3.2 The final position of the contact pairs

##### 3.2.1 Model assumptions

The analysis model is affected by many factors. Some assumptions are listed as follows:

- At beginning of the analysis, the bearing clearances only exist between bearing rollers and the outer race, in order to facilitate the analysis.
- Bearing rollers are constraint by the cage and only free in the radial direction to achieve the load equilibrium.
- Bearing rollers do not affect each other.
- The bearing clearance have no effect on the revolution speed of the bearing rollers.
- The influence of oil film on the clearance is not considered here.
- Friction and gravity are not considered.

##### 3.2.2 Inner bearing race

Based on the fixed coordinate system (the same with the coordinate system of the crank), the coordinates of the inner bearing race center  $O_{BI}$  is determined by the rotation

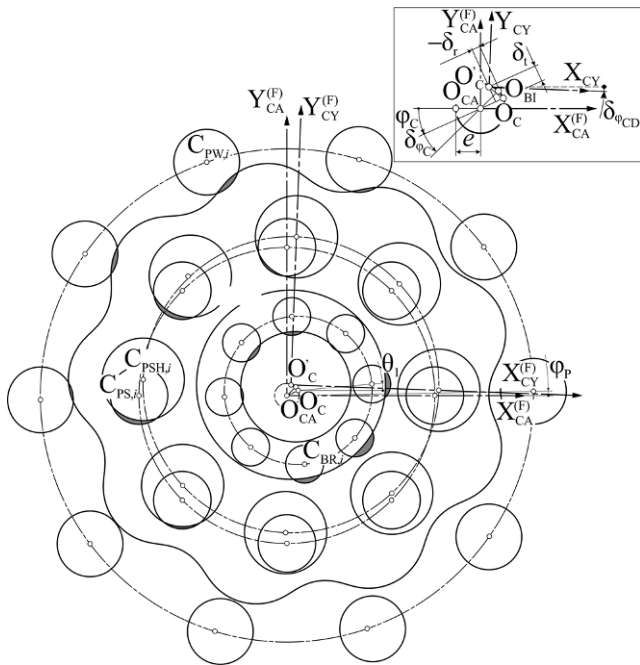


**Fig. 13** Definition the final position of each elements in the actual coordinate with four forced displacements

angle  $\varphi_C$  and the leading angle  $\delta_{\varphi_C}$  of crank due to system deformation (Fig. 13):

$$\begin{aligned} x_{O_{BI}} &= e \cos(\varphi_C + \delta_{\varphi_C}) \\ y_{O_{BI}} &= e \sin(\varphi_C + \delta_{\varphi_C}) \end{aligned} \tag{45}$$

This forced displacement will cause either a clearance or an interference between the inner race and each roller.

### 3.2.3 Cycloid disc

Because the cycloid disc owns three degrees of freedom, three forced displacements, two in translational and one in rotational, will be caused under loading. The new coordinates of the cycloid disc center  $O'_C$  are defined by the two translational displacements  $\delta_r$  and  $\delta_t$  in the fixed coordinate system (Fig. 13):

$$\begin{aligned} x_{O'_C} &= (e + \delta_{r_{CD}}) \cos \varphi_C - \delta_{t_{CD}} \sin \varphi_C \\ y_{O'_C} &= (e + \delta_{r_{CD}}) \sin \varphi_C + \delta_{t_{CD}} \cos \varphi_C \end{aligned} \tag{46}$$

In addition, the coordinate system of the cycloid disc is rotated with an angle  $\delta_{\varphi_{CD}}$  (i.e., rotational displacement) with respect to the fixed coordinate system.

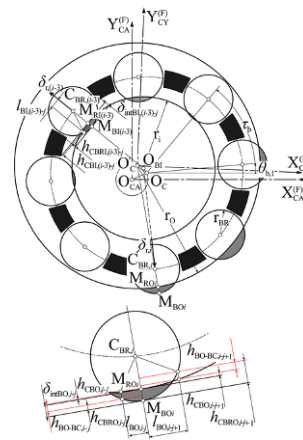


**Fig. 14** Definition the interference amount between bearing roller and inner/outer ring in the actual coordinate

### 3.2.4 Bearing rollers

The bearing rollers are placed evenly around the center of cage  $O_C$ , which is defined as:

$$\begin{aligned} x_{O_C} &= e \cos \varphi_C \\ y_{O_C} &= e \sin \varphi_C \end{aligned} \tag{47}$$

The coordinates of each roller center  $C_{BR,n}$  is (Fig. 14):

$$\begin{aligned} x_{C_{BR,n}} &= e \cdot \cos \varphi_C + (r_{BR} + r_i) \cos \theta_{b,n} \\ y_{C_{BR,n}} &= e \cdot \sin \varphi_C + (r_{BR} + r_i) \sin \theta_{b,n} \end{aligned} \tag{48}$$

where the azimuth angle  $\theta_{b,n}$  is the same in Eq. 14.

### 3.2.5 Pin-wheel

The pin-wheel is chosen here as output. The coordinates of each pin center are derived with a given output angle  $\varphi_P$  as:

$$\begin{aligned} x_{C_{PW,i}} &= R_{PW} \cos [\varphi_P + 2\pi (i - 1) / z_{PW}], \\ y_{C_{PW,i}} &= R_{PW} \sin [\varphi_P + 2\pi (i - 1) / z_{PW}]. \end{aligned} \tag{49}$$

### 3.2.6 Pin-shaft

The coordinates of each pin center  $C_{PS,i}$  of the pin-shaft are not changed with rotation of the cycloid disc, if the pin-shaft is regarded as fixed, namely from Fig. 13:

$$\begin{aligned} x_{C_{PS,i}} &= R_{PS} \cos (2\pi (i - 1) / z_{PS}) \\ y_{C_{PS,i}} &= R_{PS} \sin (2\pi (i - 1) / z_{PS}) \end{aligned} \tag{50}$$

### 3.2.7 Pin-hole

The pin-hole centers  $C_{PSH,i}$  locate equally on a circle around the cycloid disc center  $O'_C$  in the ideal case. Their coordinates are, as shown in Fig. 13:

$$\begin{aligned} x_{C_{PSH,i}} &= x_{O'_C} + R_{PSH} \cos(2\pi(i-1)/z_{PS}) \\ y_{C_{PSH,i}} &= y_{O'_C} + R_{PSH} \sin(2\pi(i-1)/z_{PS}) \end{aligned} \quad (51)$$

### 3.3 Flank separation distance of contact pairs with forced displacements

The calculation process of the separation distances in presence of clearances is not different from the process explained in Sect. 2.4, only the interference due to the forced displacement must be added into the separation distances. If the calculated interference value is positive, the separation distances are reduced with this value. If it is negative, there will be no load induced at this final position of the contact pair. This contact pair must be excluded from the LTCA calculation.

#### 3.3.1 Bearing roller

The interference between the bearing roller and the inner or outer race due to the forced displacements can be determined by using the relation of the roller center and the race center. The interference in the contact pair is illustrated in gray area (Fig. 14). The maximum value for inner race is measured along the center line of  $O_{BI}$  and  $C_{BR,i}$ , i.e.:

$$\delta_{intBI,i} = r_i + r_{BR} - \overline{O_{BI}C_{BR,i}} > 0 \quad (52)$$

Each contact point on the roller and inner race, i.e.  $M_{BI}$  and  $M_{RI}$ , respectively, can be regarded as the point on the center line  $O_{BI}-C_{BR,i}$  to determine the interference value  $\delta_{intBI,i}$ . The tangential plane can be drawn through the contact points. Therefore, the separation distance  $h_{CBI,i-j}$  of inner race and  $h_{CBRI,i-j}$  of roller are calculated based on the corresponding tangential plane as the mentioned calculation method:

$$h_{CBRI,i-j} = r_{BR} - \sqrt{r_{BR}^2 - l_{BI,i-j}^2} \quad (53)$$

$$h_{CBI,i-j} = r_i - \sqrt{r_i^2 - l_{BI,i-j}^2} \quad (54)$$

The final separation distance  $h_{BI-BC,i}$  between inner race and bearing roller for LTCA model is equal to:

$$h_{BI-BC,i} = h_{CBI,i-j} + h_{CBRI,i-j} - \delta_{intBI,i} \quad (55)$$

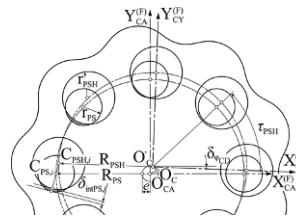


Fig. 15 Definition the interference amount between pin shafts and cycloid disc in the actual coordinate

or:

$$h_{BI-BC,i} = \overline{O_{BI}C_{BR,i}} - \sqrt{r_{BR}^2 - l_{BI,i-j}^2} - \sqrt{r_i^2 - l_{BI,i-j}^2} \quad (56)$$

In the same way, the maximum interference amount  $\delta_{intBO,i}$  between roller and outer race is:

$$\delta_{intBO,i} = \overline{O_{BO}O_{R,i}} - (r_O - r_{BR}) > 0 \quad (57)$$

The final separation distance between the outer race and the roller can be also obtained (Fig. 14) i.e.:

$$h_{BO-BC,i} = \sqrt{r_O^2 - l_{BO,i-j}^2} - \sqrt{r_{BR}^2 - l_{BO,i-j}^2} - \overline{O_{BO}C_{BR,i}} \quad (58)$$

#### 3.3.2 Hole-pin

The contact between the pin of the pin-shaft and the hole of the cycloid disc is regarded as a spring. Thus, the load acting on the pin can be derived from the interference amount  $\delta_{intPS,i}$  between the pin and the pin-hole (see Fig. 13), as the relation shows in Fig. 15, which is:

$$\delta_{intPS,i} = \overline{C_{PS,i}C_{PSH,i}} - (r_{PSH} - r_{PS}) \quad (59)$$

#### 3.3.3 Cycloid-pin

Because of the complicate cycloid tooth profile, the cycloid disc is regard as fixed here to avoid to use the coordinate transformation. The pins of pin-wheel therefore move relatively to the disc, as the relation illustrated in Fig. 16. The center of the crank  $O_{CA}$  is then changed to:

$$\begin{aligned} x_{O_{CA}}^{(CY)} &= -(e + \delta_r) \cos(\varphi_C + \delta_{\varphi_{CD}}) + \delta_t \sin(\varphi_C + \delta_{\varphi_{CD}}) \\ y_{O_{CA}}^{(CY)} &= -(e + \delta_r) \sin(\varphi_C + \delta_{\varphi_{CD}}) - \delta_t \cos(\varphi_C + \delta_{\varphi_{CD}}) \end{aligned} \quad (60)$$

The contact points on the pin-cycloid pairs are also determined based on the geometric relation, that the line  $C_{PW_i}-M_{PW_i}$  must be parallel to the normal vector  $\mathbf{n}_{M_i}$ . In other words, the normal vector  $\mathbf{n}_{M_i}$  of the contact point  $M_{PW_i}$  on

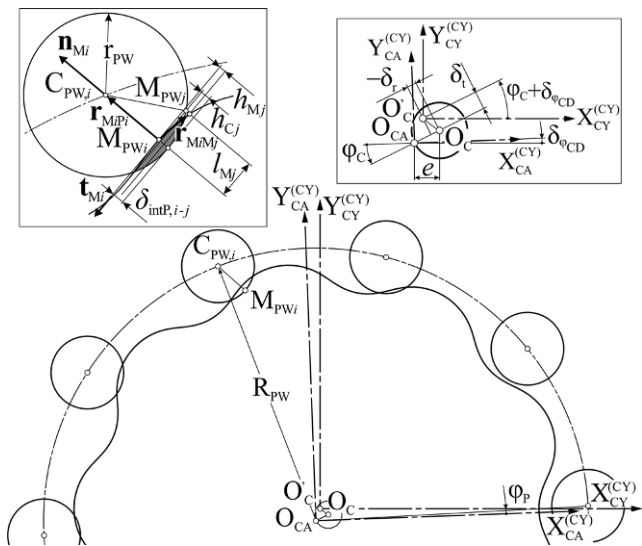


**Fig. 16** Definition the interference amount of cycloid-pin contact tooth pairs in the coordinate of cycloid disc

the cycloid disc must pass through the center of pin-wheel  $C_{PW,i}$ . The position vector  $r_{M_i P_i}$  is:

$$r_{M_i P_i} = \overline{M_{PW,i} C_{PW,i}} \cdot n_{M_i} \tag{61}$$

The pin-wheel center of  $C_{PW,i}$  represented in the cycloid coordinate system is described as:

$$\begin{aligned} x_{C_{PW,i}}^{(CY)} &= x_{O_{CA}}^{(CY)} + R_{PW} \cos \theta_{P,i} \\ y_{C_{PW,i}}^{(CY)} &= y_{O_{CA}}^{(CY)} + R_{PW} \sin \theta_{P,i} \end{aligned} \tag{62}$$

where the angle  $\theta_{P,i}$  of pin  $i$  is:

$$\theta_{P,i} = \varphi_P + \delta_{\varphi_{CD}} + 2\pi(i-1)/z_{PW} \tag{63}$$

The maximum interference amount  $\delta_{intP,i}$  between the cycloid disc and the pin-wheel is:

$$\delta_{intP,i} = r_{PW} - \overline{M_{PW,i} C_{PW,i}} \tag{64}$$

The separation distance  $h_{M_j}$  between the cycloid profile and the common tangent plane is the same with the calculation relations described in Sect. 2.4. In the same way, the separation distance  $h_{C_j}$  is also obtained. The total distance  $h_{CD-PW,i}$  for LTCA calculation is equal to:

$$h_{CD-PW,i} = h_{M_j} + h_{C_j} - \delta_{intP,i} \tag{65}$$

### 3.4 Relation of load equilibrium

The relations of load equilibrium in the case of clearance are not different from those in Sect. 2.5. Hence, the neces-

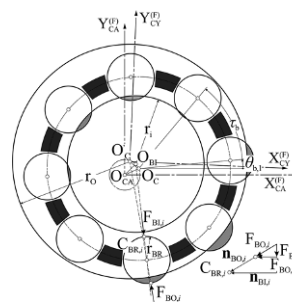


**Fig. 17** Load equilibrium relation of roller bearing in the actual coordinate

sary equations of forces on each contact tooth pair for load equilibrium is defined as follows.

#### 3.4.1 Load equilibrium of bearing roller

For each roller, the force  $F_{BO,i}$  due to contact of the outer race and roller  $i$  projected along the normal vector  $n_{BI,i}$  of the inner race must be equal to the force  $F_{BI,i}$  for inner race-roller pair (Fig. 17), i.e.:

$$F_{BI,i} = F_{BO,i} \cdot (n_{BO,i} \cdot n_{BI,i}) \tag{66}$$

The force of inner race  $F_{BI,i}$  and outer  $F_{BO,i}$  are:

$$F_{BI,i} = \sum_{j=1}^{m_I} s_{Brg,I-i} p_{Brg,I-i-j} \tag{67}$$

$$F_{BO,i} = \sum_{j=1}^{m_O} q_{Brg,O-i} p_{Brg,O-i-j} \tag{68}$$

where the coefficient  $q_{Brg,O-i}$  is equal to:

$$q_{Brg,O-i} = s_{Brg,O-i} \cdot (n_{BO,j} \cdot n_{BI,j}) \tag{69}$$

#### 3.4.2 Load equilibrium of cycloid disc

The cycloid disc is influenced by the load of bearing roller, pin shafts and pin-wheel. Those loads in the radial and the tangential direction should be in equilibrium, so as the sum of moments with respect to the center of cycloid disc. Because all forces are calculated based on the guess values of the displacements, the equilibrium conditions represented in the sum of forces are used for iterative calculation. The radial force  $F_{CY,r}$  and the tangential force  $F_{CY,t}$  in Eq. 43 can be determined as:

$$F_{CY,r} = \sum F_{BO,r} + \sum F_{PS,r} + \sum F_{PW,r} \tag{70}$$

$$F_{CY,t} = \sum F_{BO,t} + \sum F_{PS,t} + \sum F_{PW,t} \tag{71}$$

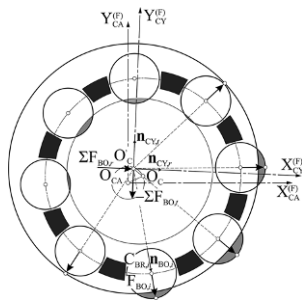


**Fig. 18** Equal load equilibrium relation of roller bearing acting on the center of outer ring

The total moment  $M_{OC}$  is also:

$$M_{OC} = M_{PW,OC} + M_{PS,OC} \tag{72}$$

The individual components of the forces and the moments in the above equations are determined as follows, see Fig. 18.

- **Loads on rollers-cycloid pair.** The forces can be decomposed into two components in different directions, i.e., tangential force  $F_{BO,t}$  and radial force  $F_{BO,r}$ . By using the vector calculation with the vector  $\mathbf{n}_{BO,i}$ ,  $\mathbf{n}_{O'C,r}$  and  $\mathbf{n}_{O'C,t}$ , we have:

$$\sum F_{BO,r} = \sum F_{BO,i} (\mathbf{n}_{BO,i} \cdot \mathbf{n}_{O'C,r}) \tag{73}$$

$$\sum F_{BO,t} = \sum F_{BO,i} (\mathbf{n}_{BO,i} \cdot \mathbf{n}_{O'C,t}) \tag{74}$$

The radial vector  $\mathbf{n}_{O'C,r}$  and tangential vector  $\mathbf{n}_{O'C,t}$  in the coordinate system of the cycloid disc are:

$$\mathbf{n}_{O'C,r} = (\cos \delta_{\varphi_{CD}}, -\sin \delta_{\varphi_{CD}}) \tag{75}$$

$$\mathbf{n}_{O'C,t} = (\sin \delta_{\varphi_{CD}}, \cos \delta_{\varphi_{CD}}) \tag{76}$$

- **Loads on pin-hole pair.** The force  $F_{PS,i}$  is produced by the interference amount  $\delta_{intPS,i}$  (Eq. 58) and stiffness  $k_{PS}$ :

$$F_{PS,i} = k_{PS} \cdot \delta_{intPS,i} \tag{77}$$

The force is directed to the center line of the pin  $C_{PS,i}$  and the hole  $C_{PSH,i}$ , i.e., the coordinates of  $C_{PSH,i}$  are:

$$\begin{aligned} x_{C_{PSH,i}}^{(CY)} &= R_{PSH} \cos \theta_{PSH,i} \\ y_{C_{PSH,i}}^{(CY)} &= R_{PSH} \sin \theta_{PSH,i} \end{aligned} \tag{78}$$

where the angle  $\theta_{PSH,i}$  is defined according to Eq. 3. The coordinates of the pin center is:

$$\begin{aligned} x_{C_{PS,i}}^{(CY)} &= x_{O_{CA}}^{(CY)} + R_{PS} \cos \theta_{PS,i} \\ y_{C_{PS,i}}^{(CY)} &= y_{O_{CA}}^{(CY)} + R_{PS} \sin \theta_{PS,i} \end{aligned} \tag{79}$$

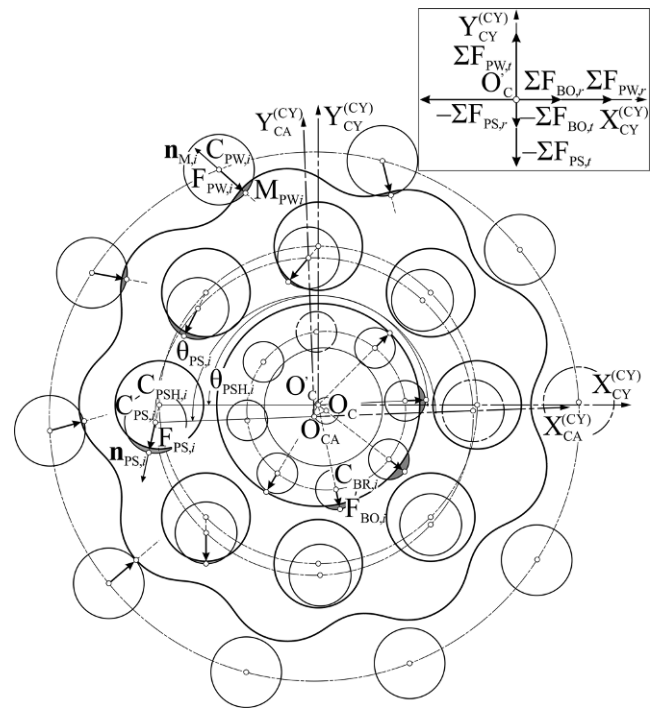


**Fig. 19** Load equilibrium relation of cycloid disc in the tangential and radial direction in the coordinate of cycloid disc

where the crank center  $O_{CA}$  can be taken from Eq. 59, the angle  $\theta_{PS,i}$  of the hole is:

$$\theta_{PS,i} = \delta_{\varphi_{CD}} + (i - 1) \tau_{PS} = \delta_{\varphi_{CD}} + 2\pi (i - 1) / z_{PS} \tag{80}$$

The direction vector  $\mathbf{n}_{PS,i}$  is:

$$\mathbf{n}_{PS,i} = C_{PS,i} \vec{C}_{PSH,i} / |C_{PS,i} C_{PSH,i}| \tag{81}$$

The radial force  $F_{PS,r}$  and tangential force  $F_{PS,t}$  on the pin is determined respectively as:

$$F_{PS,r} = \sum F_{PS,i} (\mathbf{n}_{PS,i} \cdot \mathbf{i}) \tag{82}$$

$$F_{PS,t} = \sum F_{PS,i} (\mathbf{n}_{PS,i} \cdot \mathbf{j}) \tag{83}$$

- **Load on pin-cycloid pair.** The force of each pin is:

$$F_{PW,i} = \sum_{j=1}^{m_n} s_i p_{i-j} \tag{84}$$

And the radial force  $F_{PW,r}$  and the tangential force  $F_{PW,t}$  of pin shaft (Fig. 19) can be expressed as:

$$F_{PW,r} = \sum F_{PW,i} (\mathbf{n}_{M,i} \cdot \mathbf{i}) \tag{85}$$

$$F_{PW,t} = \sum F_{PW,i} (\mathbf{n}_{M,i} \cdot \mathbf{j}) \tag{86}$$



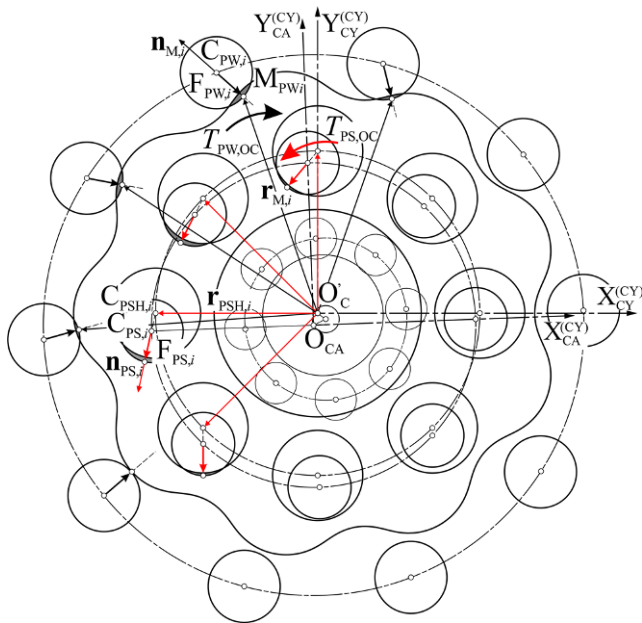


Fig. 20 Moment equilibrium relation of cycloid disc in the coordinate of cycloid disc

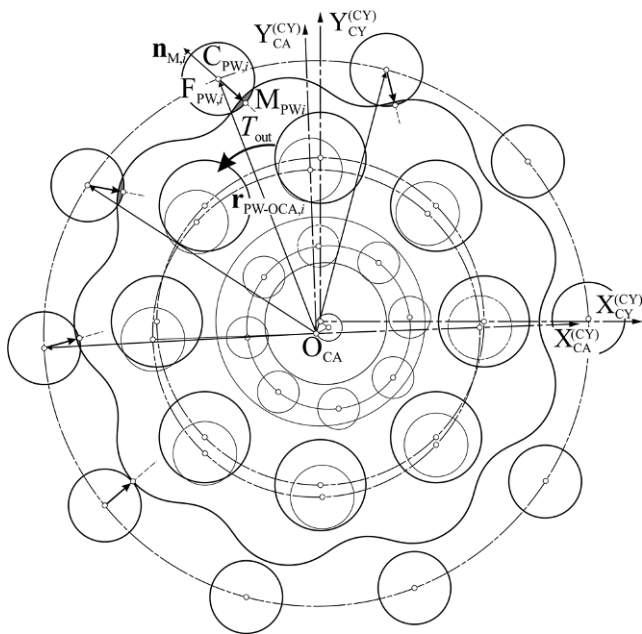


Fig. 21 Output torque equilibrium relation of pin-wheels in the coordinate of cycloid disc

- **Moments on cycloid disc.** The moment  $M_{PW,OC}$  from the pin wheel with respect to the center of cycloid disc  $O_C$  is equal to:

$$M_{PW,OC} = \sum F_{PW,i} |\mathbf{n}_{Mi} \times \mathbf{r}_{Mi}| \tag{87}$$

where  $\mathbf{n}_{Mi}$  is the direction vector for force and  $\mathbf{r}_{Mi}$  the position vector of point  $M_{PW,i}$  (Fig. 20). The moment  $M_{PS,OC}$  from the pin shaft is:

$$M_{PS,OC} = \sum F_{PS,i} |\mathbf{r}_{PSH,i} \times \mathbf{n}_{PS,i}| \tag{88}$$

### 3.4.3 Output torque equilibrium

The output torque is one boundary condition of cycloid gear drive. As a result, torque of pin wheel  $T_{PW,OP}$  with respect to the center of crank shaft should be considered, shown in Fig. 21. The torque  $T_{PW,OP}$  in Eq. 43 is equal to:

$$T_{PW,OP} = \sum F_{PW,i} |\mathbf{r}_{OCA,C_{PW,i}} \times \mathbf{n}_{Mi}| \tag{89}$$

where  $\mathbf{r}_{OCA,C_{PW,i}}$  is the position vector from the center of crank shaft  $O_{CA}$  to the pin wheel  $C_{PW,i}$ , and  $\mathbf{n}_{Mi}$  is the force vector.

### 3.5 Convergence approach for analysis model

Because the four unknown displacements are solved iteratively by using different guess values in the analysis model, it is very important to determine the new values for next step, if the convergence conditions (Eq. 43) are not met.

At the beginning of the solving process, the guess values of the displacements are obtained from the calculation of LTCA model without considering clearances, see Sect. 2. Then the sum of the loads,  $F_{CY,r}$ ,  $F_{CY,t}$ ,  $M_{OC}$ , and  $T_{PW,OP}$ , can be calculated based on the proposed LTCA model by using these displacements. Usually, the first convergence test will not be successful. The new guess values are determined by using the tangent stiffness approach, as the concept shown in Fig. 22. The new displacement  $\delta_{i+1}$  can be defined as  $\delta_i + \Delta\delta$ . The displacement difference  $\Delta\delta$  can be thus computed with the stiffness  $k$  and the load difference  $\Delta F$  between the goal value  $F_{GOAL}$  and the calculated value  $F_i$  of the force at this step:

$$\Delta\delta = \frac{\Delta F}{k} \tag{90}$$

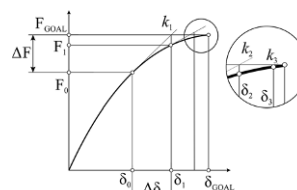


Fig. 22 Simplified tangent stiffness approach to determine a new displacement for next iteration



The tangent stiffness  $k$  can be calculated by using the finite difference method:

$$k = \frac{F(\delta_i + \varepsilon) - F_i}{\varepsilon} \tag{91}$$

This calculation approach will be repeated until  $|ΔF|$  less than the given small value.

For the problem of four variables, the individual tangent stiffness influenced by the individual displacement is applied. Thus the new displacement differences  $Δδ$  can be calculated as:

$$\begin{bmatrix} k_{r,r} & k_{r,t} & k_{r,\varphi_{CD}} & k_{r,\varphi_C} \\ k_{t,r} & k_{t,t} & k_{t,\varphi_{CD}} & k_{t,\varphi_C} \\ k_{M,r} & k_{M,t} & k_{M,\varphi_{CD}} & k_{M,\varphi_C} \\ k_{T,r} & k_{T,t} & k_{T,\varphi_{CD}} & k_{T,\varphi_C} \end{bmatrix} \begin{bmatrix} \Delta\delta_r \\ \Delta\delta_t \\ \Delta\delta_{\varphi_{CD}} \\ \Delta\delta_{\varphi_C} \end{bmatrix} = \begin{bmatrix} -F_{0,r} \\ -F_{0,t} \\ -M_0 \\ -T_0 \end{bmatrix} \tag{92}$$

where the individual tangent stiffness  $k_{ij}$  is defined as:

$$k_{i,j} = \frac{F_{i,j}(\varepsilon_{\delta j}) - F_{0,i}}{\varepsilon_{\delta j}}, \quad i : r, t, M, T; \quad j : r, t, \varphi_{CD}, \varphi_C \tag{93}$$

The next guess displacement values can be thus calculated accordingly. The calculation process is then repeated iteratively until the convergence criterion is met.

### 3.6 Loaded transmission error

In general, the (unloaded) transmission error is difficult to calculate for the case in presence of bearing clearances and/or hole-pin clearances. The rotational displacement of the crank  $\delta_{\varphi_C}$ , however, can be determined by using the proposed LTCA model. It includes an additional rotation angle due to clearances and a deformation angle. The loaded transmission error is expanded from Eq. 6 as:

$$LTE_{\varphi_C} = \varphi_{C,act} - \varphi_{C,theor} = (\varphi_C + \delta_{\varphi_C}) - u \cdot \varphi_{P,given} \tag{94}$$

The unloaded transmission error can be also obtained by using a slight torque to calculate the displacements based on the proposed LTCA model.

## 4 Analysis results for cycloid gear drive considering relevant clearances

### 4.1 Calculation data

The design data of the cyclo gear drive used in this paper for analysis are listed in Table 1. The tooth number difference of the cycloid disc is selected as 1, and only one disc is involved in the calculation. The equidistant and shifting off-

**Table 1** Essential data for numerical analysis

Items/symbols	Value	Remarks
Pitch circle radius of pin wheel $R_C$	88 mm	–
Tooth number of the cycloid disk $z_C$	13	–
Tooth number of the pin wheel $z_P$	14	–
Reduction ratio $u$ (Pin-shaft fixed)	14	$z_P/\Delta z$
Thickness of the cycloid disk $t$	11.8 mm	–
Radius of the bearing hole center $r_0$	29.5 mm	–
Pitch circle radius of the pin shaft $R_{PS}$	56 mm	–
Radius of the pin shaft hole $r_{PSH}$	14.075 mm	–
Radius of the pin shaft $r_{PS}$	10.075 mm	–
Number of pin shaft	8	–
Radius of the crank shaft $r_i$	19.5 mm	–
Radius of the bearing roller $r_{BR}$	5 mm	–
Number of bearing roller	11	–
Output torque $T$	377.3 Nm	–
Stiffness of the pin shaft	$10^6$ N/mm	–
Radius of the pin $r_P$	6.5 mm	–
Eccentricity $e$	4	–
Equidistant offset	0.15 mm	–
Shifting offset	0.09 mm	–

**Table 2** Data of relevant clearance

Case	Value of bearing clearance[mm]	Value of Pin-hole clearance[mm]
CS-1	0	0
CS-2	0.01	0
CS-3	0.03	0
CS-4	0.03	0.01
CS-5	0.03	0.02
CS-6	0.03	0.03

set modification are used for the cycloid tooth profile which yield about 10 arcmin of backlash. Three different amounts of bearing clearance and pin-hole clearance, Table 2, are used to analyze their effects on the contact characteristics, where six different cases of combination are considered for analysis.

### 4.2 Loaded transmission error

The analysis results of transmission error (TE) considering bearing and pin-hole clearances are shown in Fig. 23, where a slight output torque in value of 10 Nm, about 3% of full output torque (377.3 Nm), is applied for calculation. If only the bearing clearance is considered, not only the variation of TE, but the peak-to-peak value of TE (PTPTE) is changed slightly with an enlarged bearing clearance (CS-1 to CS-3). But the influence of the hole-pin clearance is significant. The PTPTE value is enlarged as the pin-hole clearance, see the variation in the cases CS-3 to CS-6. However, the trend of the variation of TE due to the pin-hole clearance changes

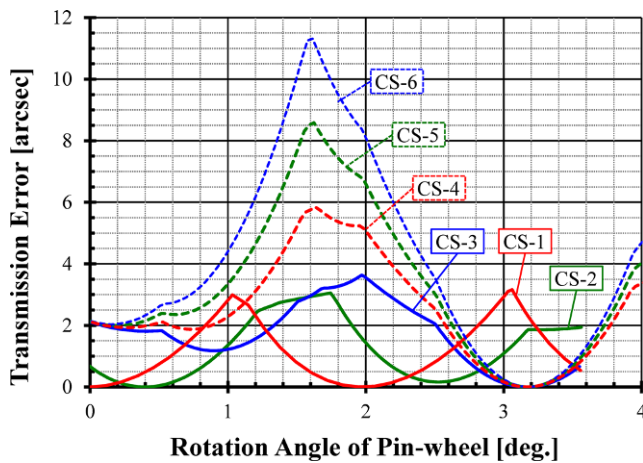


Fig. 23 Transmission error of cases of relevant clearances

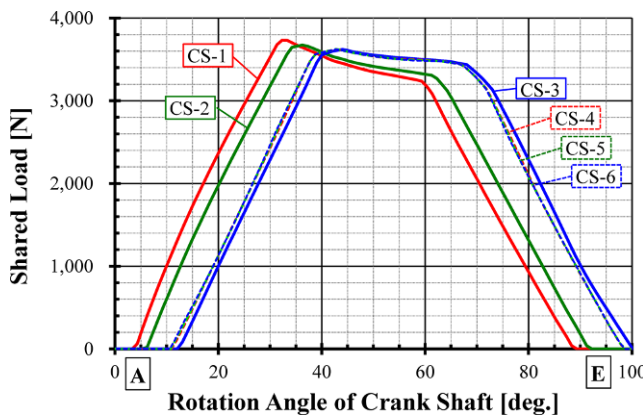


Fig. 24 Shared loads on the cycloid flanks for cases of relevant clearances

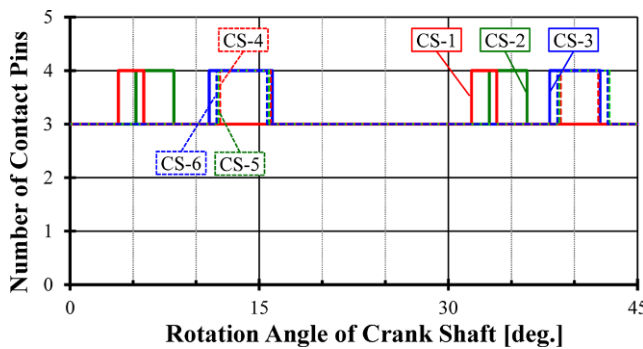


Fig. 25 Number of contacts pin-wheel-cycloid pairs under load

little, in comparison of the influence of bearing clearance. In addition, the periods of TE due to the clearances (CS-2 to CS-6) become larger than the case without clearance (CS-1), here about 2 deg ( $= 360^\circ/13/14$ ).

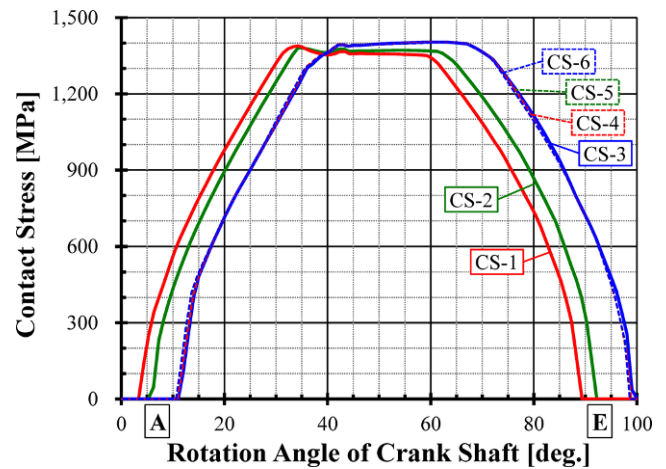


Fig. 26 Contact stress on the cycloid flanks for cases of relevant clearances

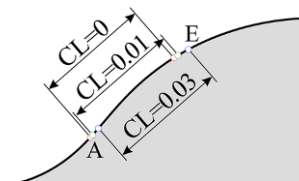


Fig. 27 Contact area of pin-wheel contact tooth pairs in different cases of bearing clearance

### 4.3 Shared loads of pin-wheel on cycloid flank

The variation of the normal load acting on the individual cycloid flank during the mesh cycle, is illustrated in Fig. 24. It is clearly to find that the begin of contact will be more delayed as the bearing clearance increases. This effect due to the bearing clearance (CS-2 and CS-3) is stronger than that due to the pin-hole clearance (CS-4 to CS-6). Additionally, the maximum load on cycloid flank is reduced only around 3% due to a larger bearing clearance (CS-3). However, this reduction is not significant in the cases with pin-hole clearances. The reason for this effect is the variation of the number of contact as the diagram illustrated in Fig. 25. It can be seen clearly that the larger bearing clearance will enlarge the contact ratio (CS-1 to CS-3), while the pin-hole clearance has less influence (CS-4 to CS-6).

### 4.4 Contact stress of pin-wheel acting on an individual cycloid flank

The variation of the contact stress on an individual flank for the six cases is illustrated in Fig. 26. The difference among the results of the various cases is small, especially the influence of the pin-hole clearance is small enough to be ignored. Although the maximum shared load in CS-3 is smaller than the other, the maximum contact stress in CS-3 is slightly enlarged in 1% in comparison with CS-1 (clearance-free). This can be explained with aid the contact zone on the modified flank (Fig. 27). The contact zone of

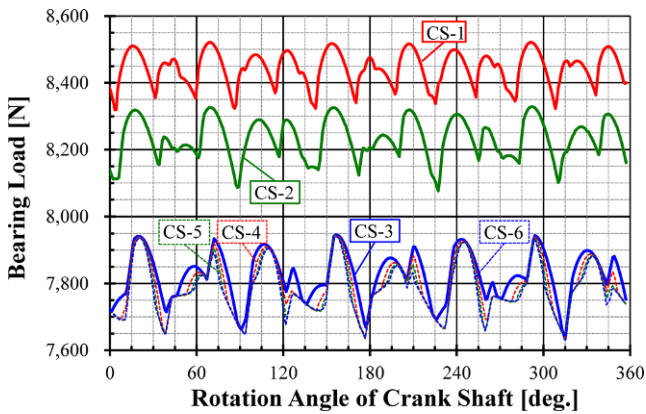


**Fig. 28** Bearing loads on the cranks of cases of relevant clearances

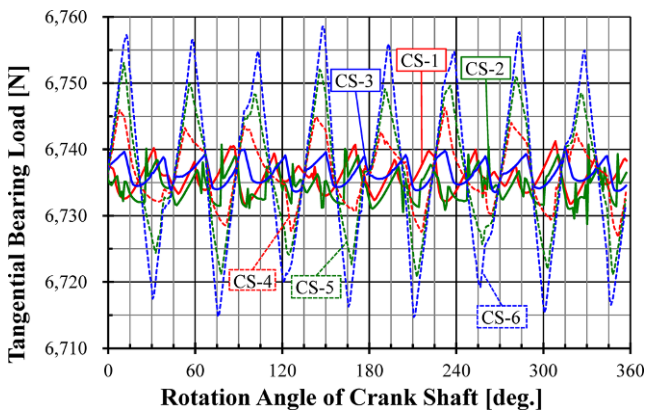


**Fig. 29** Tangential bearing loads on the cranks of cases of bearing clearance

the case CS-3 will be shifted towards to the tip of cycloid tooth, where a larger curvature is expected.

### 4.5 Loaded characteristics on the crank

It is interesting to explore the influences of clearances on the contact characteristics of the crank bearing.

#### 4.5.1 Bearing loads

At first, it can be seen from Fig. 28 clearly that the average bearing load drops slightly as the bearing clearance increases, while the peak-to-peak value is enlarged accordingly. The difference between the case CS-1 and CS-3 is about 550 N (6.5% of 8460 N). On the other hand, the pin-hole clearance has less influences on the bear load. The bearing load can be divided into the tangential and radial force.

In general, the tangential bearing force remains constant with a contact output torque  $T_{out}$  under ideal condition. However, it varies with the rotating angle due to transmission error (Fig. 29). Additionally, the average value of

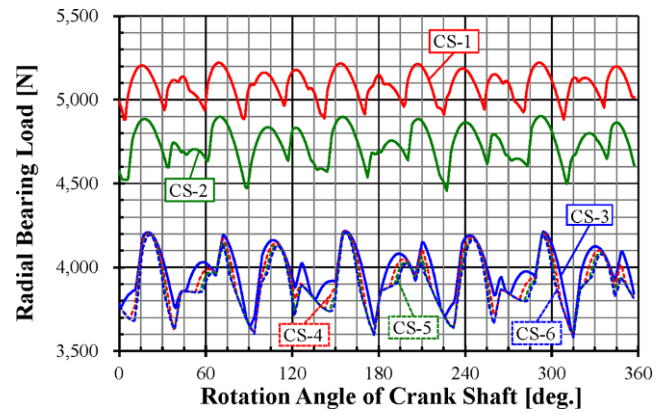


**Fig. 30** Radial bearing loads on the cranks of cases of bearing clearance

the tangential bearing load remains with the various cases of clearances, while the peak-to-peak value increases with enlarged clearances. Especially the pin-hole clearance has more influence than the bearing clearance, although the maximal PTP-value in the analysis example is less than 45 N (0.66% of 6737.5 N).

On the other hand, the variation of the radial bearing force (Fig. 30) shows a similar trend with the total load, because the variation of the tangential loads is small.

#### 4.5.2 Distribution of load and contact stress on individual roller

In case of non-modified roller profile, the stress concentration can be found clearly near the end face of the roller, as the saddle-shaped distribution of contact stress in the diagram of Fig. 31 shows. The saddle-shape of stress distribution can be seen in all cases with different bearing and pin-hole clearances. The diagrams of 3D-stress distribution for the other cases are therefore not shown here. Instead, the diagram in Fig. 32 shows the variation of the contact stress along the major axis of the contact pattern for various cases of clearances. And the variation of the contact stress along the minor axis is shown in Fig. 33. The weak influences of the pin-hole clearance on the contact stress of roller can be clearly identified. Although the average bearing load is reduced with larger clearances, refer to Fig. 28, the maximum load acting on an individual roller increases due to reduced contact zone of the bearing roller (Fig. 34). The contact stress of the case with a larger bearing clearance (CS-6) is then larger than the other. However, the effect of the pin-hole clearance is very small.

#### 4.6 Pin shaft loads

The loads acting on the cycloid disc, which come from three types of contact pairs, will affect each other. From this point

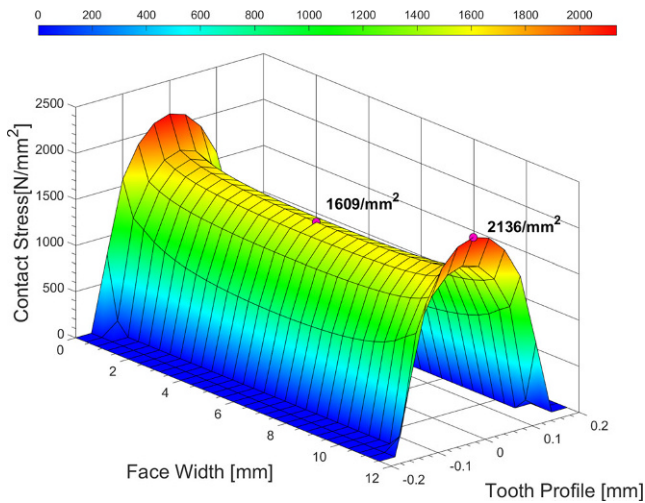


**Fig. 31** Contact stress distribution for bearing clearance=0.03 mm, CS-3

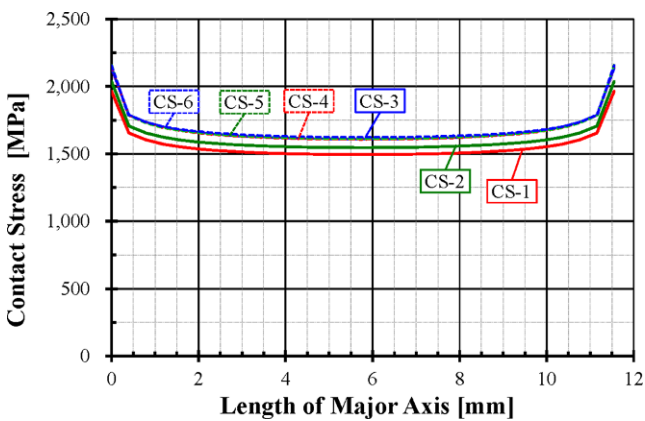


**Fig. 32** Contact stress distribution along the major axis for various cases of clearances

of view, the influence of the bearing and pin-hole clearances on the pin shaft loads can be clearly explained. Because the clearances have less influences on the loads acting on the cycloid flanks, the pin-hole loads have a strong relationship with the bearing loads. Therefore, the maximum pin-shaft load is enlarged as the bearing clearance increases, i.e., from 5252 N in CS-1 to 6256 N in CS-3 (Fig. 35) while the bearing load is reduced accordingly (Fig. 28). The pin-hole clearances, on the other hand, have less effect, just like the effect on the bearing loads. However, the pin-hole clearances change the variation the shared load, as the plateau range in the curve (Fig. 35) shows. In addition, the contact range the pin is also reduced with a larger bearing and pin-hole clearances, namely from about  $98^\circ$  in CS-1 to  $62^\circ$  in CS-6. The reason for this effect can be explained based on the variation of the contact number of pins (Fig. 36). The contact ratio of the pins with the disc-hole is reduced with a larger clearance. As the pin-hole clearance is present (CS-

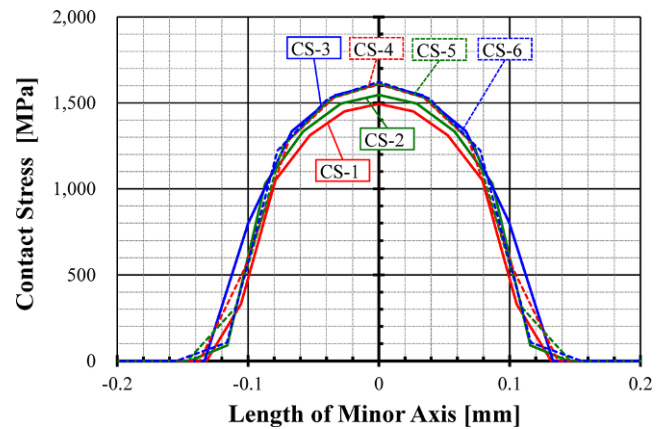


**Fig. 33** Contact stress distribution along the minor axis for cases of clearances

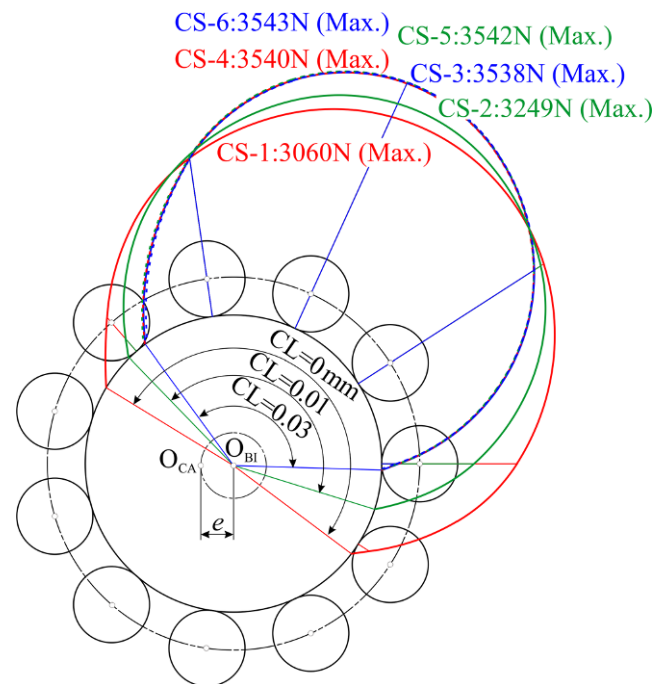


**Fig. 34** Load distribution of bearing rollers acting on the crank shaft for cases of bearing clearance

4), the contact ratio drops drastically. But it is changed less, as the pin-hole clearance increases (CS-5 and CS-6).

### 5 Conclusion and outlook

In order to explore the influence of relevant clearances on the contact characteristics in so-called Cyclo-reducers, a new computerized LTCA model based on influence coefficient method is proposed. The influence analysis of the clearance is conducted with an example from industry. Three different bearing clearances, 0, 0.01 and 0.03 mm, and three different hole-pin clearances, 0.01, 0.02 and



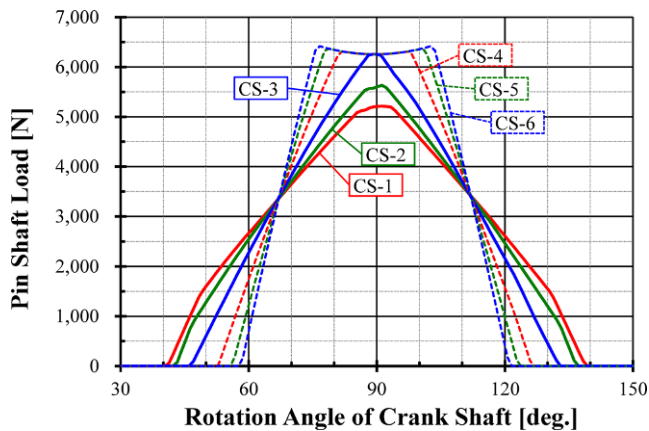


Fig. 35 Shared load of pin shaft for cases of relevant clearances

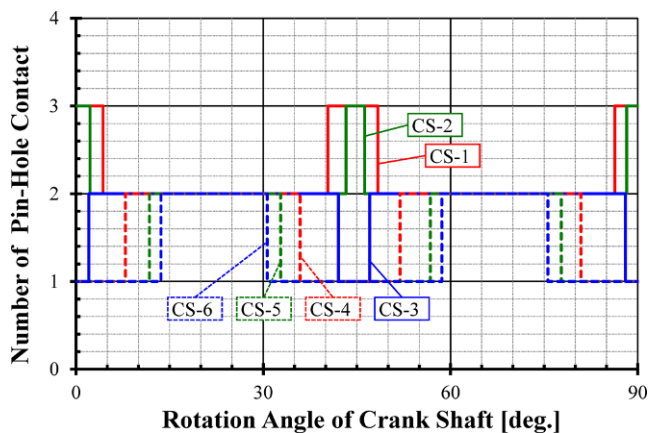


Fig. 36 Number of contacts hole-pin-cycloid pairs under load

0.03 mm, are used in the calculation. The analysis results, including transmission error, loaded conditions in various contact pairs, enable us to draw some conclusions:

- The bearing clearance has no significant effect on the transmission error. The peak-to-peak value of loaded transmission error in the case of bearing clearance 0.03 mm slightly increase from about 3.2 arcsec to 3.7 arcsec. But the peak-to-peak value is affected significantly by the pin-hole clearance. For example, the value in the case with a pin-hole clearance 0.03 mm and a bearing clearance 0.03 mm is about two times larger than that only considering bearing clearance 0.03 mm.
- The bearing clearance and the hole-pin clearance have less effects on the shared load and the contact stress on an individual cycloid flank. The maximum shared load is reduced only about 3% in the case of bearing clearance 0.03 mm, while the maximum contact stress is enlarged about 1% in the same case.
- The contact of the pin with the cycloid tooth will delay due to presence of clearance. In this example the delayed angle is about 10 degrees in the case of a bearing

clearance 0.03 mm, and 2 degrees of a bearing clearance 0.01 mm. But the influence of the pin-hole clearance is very little.

- The bearing clearance has moderate effect on the bearing loads. The average bearing load reduces about 6.5% due to the bearing clearance of 0.03 mm, while the tangential load increases about 0.2%, and the radial load reduces about 20% in the same case. However, the pin-hole clearance has little influence. Although it can cause a larger peak-to-peak value of the variation of the tangential bearing load than the bearing clearance, the maximum value is only 0.66% of the average tangential bearing load.
- The maximum shared load and the maximum contact stress on an individual roller are enlarged as the bearing clearance increases, because the contact zone of the bearing rollers is reduced accordingly. The pin-hole clearance has also very little influence.
- The bearing clearance has strong effect on the loads acting on the pin shaft. The shared load on an individual pin increases about 20% due to the clearance with the value of 0.03 mm. However, as the pin-hole clearance increases, the maximum load does not change significantly, and is only enlarged with an increment of about 3%. A plateau range in the variation curve of the pin load can be found.

The analysis results can verify that the proposed computerized LTCA approach is an efficient simulation tool for designing Cyclo-reducer with modified flanks considering the bearing clearance and pin-hole clearance. It is thus expected to further develop a complete model considering all the relevant errors.

**Funding** The authors would like to thank the Ministry of Science and Technology, Taiwan (MOST 109-2221-E-008-001-) and Transmission Machinery Co., Ltd., Taiwan for their financial support.

## References

1. Transmission Machinery Co., Ltd., <http://www.transcyko-transtec.com/>. 2021
2. Braren LK (1928) Gear transmission. US Patent 1694031A, USA
3. Hong SW, Tong VC (2016) Rolling-element bearing modeling: a review. *Int J Precis Eng Manuf* 17:1729–1749. <https://doi.org/10.1007/s12541-016-0200-z>
4. Harris TA, Kotzalas MN (2006) Essential concepts of bearing technology. CRC Press, Taylor & Francis Group, Boca Raton, USA
5. Ji P, Gao Yuan MF, An Q (2015) Influence of roller diameter error on contact stress for cylindrical roller bearing. *Proc Inst Mech Eng Part J J Eng Tribol* Vol 229(6):689–697. <https://doi.org/10.1177/1350650114559617>
6. Filetti EG, Rumbarger JH (1970) A General method for predicting the influence of structural support upon rolling element bearing performance. *J Lubric Tech-T ASME* 92(1):121–127. <https://doi.org/10.1115/1.3451289>

7. Bourdon A, Rigal JF, Play D (1999) Static rolling bearing models in a CAD environment for the study of complex mechanisms part II—complete assembly model. *ASAE. J Tribol* 121(2):215–223. <https://doi.org/10.1115/1.2833924>
8. Szuminski P (2007) Determination of the stiffness of rolling kinematic pairs of manipulators. *Mech Mach Theory* 42:1082–1102. <https://doi.org/10.1016/j.mechmachtheory.2006.09.009>
9. Edwin LJ (2011) Numerical model to study of contact force in a cylindrical roller bearing with technical mechanical event simulation. *J Mech Eng Autom* 1:1–7. <https://doi.org/10.5923/j.jmea.20110101.01>
10. Qian W (2018) Dynamic simulation of cylindrical roller bearings. Doctoral thesis of. RWTH Aachen, University
11. Kabus S, Hansen MR (2014) Mouritsen Oφ. A New Quasi-static Multi-degree Freedom Tapered Roll Bear Model To Accurately Consider Non-hertzian Contact Press Time-domain Simulation *P I Mech Eng K—j Mul* 228:111–125. <https://doi.org/10.1177/1464419313513446>
12. Xu LX, Yang YH (2016) Dynamic modelling and contact analysis of a cycloid-pin gear mechanism with a turning arm cylindrical roller bearing. *Mech Mach Theory* 104:327–349. <https://doi.org/10.1016/j.mechmachtheory.2016.06.018>
13. Xu LX, Chen BK, Li CY (2019) Dynamic modelling and contact analysis of bearing-cycloid-pinwheel transmission mechanisms used in joint rotate vector reducer. *Mech Mach Theory* 137:432–458. <https://doi.org/10.1016/j.mechmachtheory.2019.03.035>
14. Huang J, Li C, Chen B (2020) Optimization design of RV reducer crankshaft bearing. *Appl Sci*. <https://doi.org/10.3390/app10186520>
15. Tsai SJ, Huang CH, Yeh HY, Huang WJ (2015) Loaded tooth contact analysis of cycloid planetary gear drives. *Proc. IFToMM 14th World Congress*. <https://doi.org/10.6567/IFToMM.14TH.WC.OS6.014>
16. Tsai SJ, Huang WJ, Huang CH (2015) A computerized approach for load analysis of planetary gear drives with epitrochoid-pin tooth-pairs. *VDI-Berichte* 2255(1):307–317
17. Huang CH, Tsai SJ (2017) No.6. A Study on loaded tooth contact analysis of a cycloid planetary gear reducer considering friction and bearing roller stiffness. *J Adv Mech Des Syst* .11, vol 11. <https://doi.org/10.1299/jamdsm.2017jamdsm0077>
18. Chang LC, Tsai SJ, Huang CH (2019) A study on tooth profile modification of cycloid planetary gear drives with tooth number difference of two. *Forsch Ingenieurwes* 83:409–424. <https://doi.org/10.1007/s10010-019-00355-4>
19. Tsai SJ, Chang LC, Huang CH (2017) Design of cycloid planetary gear drive with tooth number difference of two. *Forsch Ingenieurwes* 81:325–336. <https://doi.org/10.1007/s10010-017-0244-y>
20. Wu SH, Tsai SJ (2009) Contact stress analysis of skew conical involute gear drives in approximate line contact. *Mech Mach Theory* 44:1658–1676. <https://doi.org/10.1016/j.mechmachtheory.2009.01.010>